Electric Power Systems Research 229 (2024) 110119

Contents lists available at ScienceDirect

Electric Power Systems Research

journal homepage: www.elsevier.com/locate/epsr

Single-cycle P Class phasor estimation based on harmonics whitening and off-nominal frequency offset adjustment

David Macii [a,*], Amir Bashian [a], Xuansheng Shan [a,b], Daniele Fontanelli [a], He Wen [b], Dario Petri [a]

[a] Department of Industrial Engineering, University of Trento, 38123, Trento, Italy
[b] College of Electrical and Information Engineering, Hunan University, 410082, Changsha, China

ARTICLE INFO

Keywords:
Power system measurements
Phasor measurement units (PMUS)
Harmonics rejection
Protection equipment

ABSTRACT

Phasor Measurement Units (PMUs) are essential for real-time power system monitoring and control. In this paper, a novel algorithm for protection (i.e., P Class) PMUs is presented. The proposed algorithm consists of four steps: preliminary narrowband disturbance whitening; estimation of the off-nominal fundamental frequency offset through the Interpolated Discrete Time Fourier Transform (IpDFT); data record length adjustment to refine narrowband disturbance whitening over an integer number of fundamental periods; time-domain estimation of the Taylor's series coefficients of the synchrophasor function through a weighted least-squares estimator (after correction of possible static off-nominal deviations). The key novel contribution of the proposed approach is its superior ability to smooth harmonic disturbances over shorter observation intervals than many existing algorithms (which typically require at least two-cycle-long data records to meet P Class accuracy requirements), while ensuring a good tracking capability of transient events with a reasonable execution time. Several simulation and experimental results confirm that, in the case of multi-harmonic distortion, the proposed approach returns more accurate results than both the basic Taylor-series-based Weighted Least-Squares (TWLS) estimator and other whitening-based techniques, while ensuring compliance with P Class specifications even over one-cycle-long data records.

1. Introduction

Phasor Measurement Units (PMUs) play a crucial role in Wide Area Monitoring Systems (WAMS) [1], e.g., for fault location [2–4], enhanced and secure system observability [5], as well as robust system state estimation even in the presence of contingencies [6], time-varying operating conditions (e.g., due to large photovoltaic penetration) [7], and when bad data are collected [8]. In general, the PMUs are required to measure AC voltage or current amplitude, phase, frequency, and rate of change of frequency (ROCOF) at times synchronized with the Coordinated Universal Time (UTC), and to transfer them to the so-called Phase Data Concentrator (PDC) at rates between 10 frame/s and 100 or 120 frame/s depending on whether the nominal power system frequency is 50 Hz or 60 Hz. Sometimes, the possible decaying DC offsets affecting voltage or current waveforms after a fault are also included among the quantities to be measured [9]. Moreover, the real-time accurate measurement of frequency and ROCOF has become increasingly important to monitor system stability and for fast frequency support when low-inertia, renewable-based distributed generators are connected to the grid through smart power converters [10].

In the IEC/IEEE Standard 60255–118–1:2018 [11], various Total Vector Error (TVE), Frequency Error (FE) and Rate of change of Frequency Error (RFE) limits are specified in both steady-state and dynamic testing conditions. Such conditions and the related limits are divided into two categories, i.e., the *P Class* ones (mainly oriented to protection purposes) and the *M Class* ones, that are more suitable for monitoring applications.

In *P Class* PMUs, a good trade-off between measurement latency and accuracy is needed to promptly trigger protection devices and/or to support possible control strategies effectively. Therefore, measurements over short data records (usually no longer than about two fundamental periods) have to be performed to ensure that latency is low enough. On the contrary, in the *M Class* PMUs, longer data records are needed to achieve high accuracy even under severe and strongly off-nominal operating conditions. In this case, the higher measurement latency is due not only to the larger amount of samples to be processed, but also to the phase delay of the filters used to extract the signal parameters of interest [12]. For instance, in Annex D of [11] synchrophasors are

* Corresponding author.
E-mail address: david.macii@unitn.it (D. Macii).

https://doi.org/10.1016/j.epsr.2024.110119
Received 1 August 2023; Received in revised form 7 December 2023; Accepted 3 January 2024
Available online 9 January 2024

estimated through the direct demodulation of AC waveforms followed by low-pass filtering of the in-phase and quadrature components. This technique is implemented in several commercial PMUs, but it requires digital Finite Impulse Response (FIR) filters with impulse responses with length of several fundamental periods to ensure a frequency response with both a narrow transition bandwidth and a large stopband attenuation [13]. Such requirements become even stricter if the filter passband has to be enlarged to avoid excessive attenuation of phasor oscillations [14], or whenever first- and second-order differentiators are used to compute frequency and ROCOF from phase angle values [15], due to the high sensitivity of frequency and ROCOF estimators to input noise [16]. Moreover, the ROCOF measurements, although critical for grid control, monitoring and protection, can be hardly estimated with standard linear techniques during step-like transients [17].

Similar remarks generally apply also to most of the frequency-domain estimators for PMUs, e.g., the Interpolated Discrete Fourier Transform (IpDFT) [18], the iterative IpDFT (which can compensate for the effect of low-order single harmonics and interharmonics) [19,20], and the Interpolated Dynamic Discrete Fourier Transform (IpD2FT) [21]. Better results can be obtained through compressive sensing techniques applied to a Taylor-Fourier multifrequency model (especially when interharmonics are considered), but the performance over one-cycle-long intervals is not clear [22].

In this paper instead, an algorithm able to provide high synchrophasor estimation accuracy for *P Class* PMUs over short data records affected by a significant harmonic distortion is proposed. The algorithm relies on the following steps: i) narrowband whitening; ii) IpDFT-based preliminary estimation of the average fundamental frequency; iii) data record length adjustment with a further refinement of disturbance whitening and iv) tuned weighted least-squares estimation of the Taylor's series coefficients of the dynamic synchrophasor function. Thus, the proposed solution is called Whitening-based, IpDFT-driven Taylor's series Weighted Least-Squares (WI-TWLS) estimation algorithm.

In the rest of this paper, after a deeper explanation of the novelty of the proposed approach (Section 2), the steps of the algorithm are described and justified in Section 3. Section 4 reports a simulation-based comparative analysis of algorithm performance in a variety of testing conditions (especially, in the *P Class* case, as reported in [11]). Section 5 presents some interesting experimental results both under the effect of multiple stationary harmonics and during fast transient conditions measured on the field. Finally, Section 6 concludes the paper.

2. Related work

The problem of fast synchrophasor and frequency tracking in non-stationary conditions has been widely investigated over the last ten years. The fact that synchrophasors are regarded as time-varying quantities led many researchers to explore the possibility to use dynamic estimators (particularly different kind of nonlinear Kalman filters) to track sudden changes of ac waveform amplitude, frequency and ROCOF [23,24]. Among them, the use of the unscented transform combined with a Kalman filter proved to be particularly effective, since the measurement model for phasor estimation is nonlinear and the process and measurement noises not always can be assumed to be normally distributed [25–27]. Unfortunately, despite the excellent behavior of such estimators under dynamic conditions, they are usually strongly affected by harmonic and inter-harmonic distortion [28]. This problem can be partially addressed either including the harmonics phasors in the state vector [29], or smoothing narrowband disturbances through a prior decorrelation [30].

The proposed algorithm provides a higher harmonics rejection, as it relies on the same Taylor's series Weighted Least-Squares (TWLS) estimator that was conceived to track single or multi-harmonic phasor oscillations over time (particularly amplitude and phase oscillations) [31,32]. However, unlike the original least-squares estimator presented in [33], in the TWLS a weight matrix is used to smooth the errors affecting the Taylor's series coefficients estimation due to the discontinuities at the ends of each observation interval. The application of standard window functions (e.g., the Kaiser window or the Hann window) can indeed provide a significant reduction of the worst-case TVE values in the vast majority of the testing conditions described in the IEEE/IEC Standard [34]. To reduce the computational complexity, an efficient variant of the original method to estimate the fundamental component is proposed in [35].

However, when both accuracy and responsiveness are required, the synchrophasor estimation algorithm should be able to counteract the effect of multiple harmonics with a reasonable tracking capability of the fundamental. The detrimental effect of possible harmonics can be mitigated through the so-called Taylor-Fourier Transform (TFT) which extends the Taylor's series model to a given number of harmonic components, thus reducing their impact on the estimation of the fundamental parameters [32]. The measurement errors due to possible unknown static off-nominal fundamental frequency deviations can be reduced if the fundamental frequency is measured to compute the coefficients of the systems of equations of the TWLS-based estimator including a lower number of harmonics in the system model [36]. This approach is adopted in this paper too, but the impact on frequency estimation uncertainty of the preliminary IpDFT stage is strongly attenuated by a disturbance whitening transformation. Moreover, the impact of narrowband disturbances on synchrophasor estimation over very short data records (consisting of one or two fundamental periods) is mitigated by a linear transformation that tends to transform the narrowband components other than the fundamental into white noise. The feasibility of this idea, which relies on signal and noise subspace decomposition of multi-tone, real-valued signals embedded into white noise [37], was investigated for the first time in [38], and it was later successfully applied to a Taylor-Kalman Filter (TKF) for *P Class* PMUs [30].

In the following, it is shown that the best tradeoff between accuracy improvement, responsiveness and computational burden is achieved when one-cycle-long data record are considered. This result is remarkable, since the FIR filters for *P Class* PMUs based on the in-phase/quadrature demodulation of the collected waveform (as described in Annex D of the IEEE/IEC Standard) can hardly provide adequate rejection to harmonics if the filter impulse response is shorter than two or three fundamental cycles [13]. In fact, even the solutions based on the cascade of one-cycle-long FIR adaptive filters exhibit a two-cycle-long impulse response [39].

The algorithm proposed in this paper inherits some of the basic features of the solution described in [30] (most notably the idea of combining disturbance whitening with frequency adjustment), but with two major advantages, i.e., i) a lower sensitivity to narrowband disturbances than the TKF; ii) a lower computational burden for the same number of processed samples. Moreover, even if the use of dynamic Kalman-based estimators is often a preferable choice to track the variation of voltage or current components over time [40], in this paper it will be shown that an estimator based on the TWLS approach exhibits comparable responsiveness and accuracy during real transient events, but with better noise and harmonics rejection capabilities, as it will be shown in Section 5. As a result, the obtained measurement data can be successfully used to feed other cascaded protection-oriented algorithms (e.g., for islanding detection). Also, the use of cleaner data is preferable if such algorithms are particularly sensitive to disturbances, e.g., when the Teager-Kaiser energy operator is used [41].

3. Estimation algorithm description

The AC current or voltage signals collected by a PMU can be modeled with the following function:

$$s(t) = x(t) + d(t) + \varepsilon(t) = a(t)\cos(2\pi f_0 t + \varphi(t)) + d(t) + \varepsilon(t), \quad (1)$$

where

- $a(t)$ is the time-varying amplitude of the AC fundamental component $x(t)$;
- $\varphi(t)$ represents the time-varying phase fluctuations of the fundamental (obviously, in steady-state, ideal operating conditions $\varphi(t) = \varphi_0$);
- $f_0 = f_{nom}\cdot(1+\delta)$ is the fundamental frequency that in general differs from the nominal value f_{nom} by a factor δ, which is usually in the order of a fraction of percent and in any case it must not exceed a few percent points.
- The function

$$d(t) = \sum_{d=1}^{D} a_d \cos(2\pi f_d t + \varphi_d), \tag{2}$$

includes D significant harmonic and interharmonic interferers of amplitude a_d, frequency f_d and initial phase φ_d, respectively, overlapped to the fundamental.

- Finally, $\varepsilon(t)$ is the broadband, normally distributed noise floor with zero-mean and variance $\sigma_\varepsilon{}^2$.

Assuming that the phasor of $x(t)$ is measured at a UTC reference time t_r (with r being a non-negative integer), then the synchrophasor is defined as [11]

$$p(t_r) = \frac{a(t_r)}{\sqrt{2}} e^{j\varphi(t_r)}, \tag{3}$$

and the corresponding fundamental frequency and ROCOF are given respectively by

$$f(t_r) = f_0 + \frac{1}{2\pi}\frac{d\varphi(t)}{dt}\bigg|_{t_r}, \tag{4}$$

$$ROCOF(t_r) = \frac{df}{dt}\bigg|_{t_r} = \frac{1}{2\pi}\frac{d^2\varphi(t)}{dt^2}|_{t_r}. \tag{5}$$

If an integer number of samples is collected in a nominal period, i.e., $M = f_s / f_{nom}$ (where f_s is the PMU sampling rate) and C denotes the number of nominal fundamental periods that are collected by the PMU to return a single estimate of synchrophasor, frequency and ROCOF, the total number of samples within a single data record is $N = M{\cdot}C$.

When estimators based on the Taylor's series of the phasor function are considered, it is a common practice to choose the reference time t_r approximately in the center of the r^{th} data record. In this way, the Taylor's series truncation error is minimum [33,34]. Therefore, recalling that: i) t_r is synchronized to the UTC and ii) the sampling clock is disciplined accordingly, then $r = t_r{\cdot}f_s$ and the samples of the r^{th} data record can be indexed by variable n_r, with $r - \frac{N-1}{2} \le n_r \le r + \frac{N-1}{2}$ or $r - \frac{N}{2} \le n_r \le r + \frac{N}{2} - 1$ depending on whether N is an odd or an even number, respectively. In both cases, the collected samples can be gathered into a single N-long column vector $\boldsymbol{s}_r$. In the following, with no loss of generality, N will be assumed to be odd. In this way, t_r lies exactly in the center of the r^{th} observation interval. Fig. 1 shows the flowchart of the WI-TWLS algorithm to estimate the values of (3)–(5) using the data within vector $\boldsymbol{s}_r$.

3.1. Narrowband disturbance whitening

The aim of the first step of the WI-TWLS algorithm is to remove (or at least to strongly attenuate) the narrowband disturbances modeled by (2) with a negligible impact on the fundamental component $x(t)$ in (1). To this end, assuming that $(D + 1) < N/2$ (a condition that is easily met in practice), it can be shown (see for instance [37]) that the Singular Value Decomposition (SVD) of the $N \times N$ autocorrelation matrix of $\boldsymbol{s}_r$ can be expressed as follows, i.e.

$$Q_r = E(\mathbf{s}_r{\cdot}\mathbf{s}_r^T) = S_r \begin{bmatrix} \Lambda_0 & 0 \\ 0 & \widetilde{\Lambda}_0 \end{bmatrix} S_r^T = S_r \begin{bmatrix} \Lambda_0 & 0 & 0 \\ 0 & \Lambda_D & 0 \\ 0 & 0 & \sigma_\varepsilon^2 I_{N-2D-2} \end{bmatrix} S_r^T, \tag{6}$$

where:

- $E(\cdot)$ is the expectation operator;
- The columns of matrix S_r (of size $N \times N$) are the orthonormal singular vectors of Q_r;
- The 2×2 diagonal matrix Λ_0 includes the singular values of the fundamental component;
- $\widetilde{\Lambda}_0$ is a diagonal matrix that comprises both the singular values of the narrowband components other than the fundamental and those associated with the wideband noise floor;
- Submatrix Λ_D contains only the D pairs of singular values associated with harmonics and interharmonics;
- $I_{N\text{-}2D\text{-}2}$ is the identity matrix that, multiplied by $\sigma_\varepsilon{}^2$, returns the singular value matrix of the noise subspace of dimension N-2D-2.

It is worth noticing that since matrix Q_r is positive semidefinite, the singular values and the eigenvalues Q_r (as well as the singular vectors and the eigenvectors of Q_r) coincide. Therefore, in the following terms such as singular values and eigenvalues or singular vectors and eigenvectors will be used as synonyms.

Recalling that the eigenvalues in Λ_0 and Λ_D are proportional to the power of the respective real-valued sinusoidal components [37,38], the

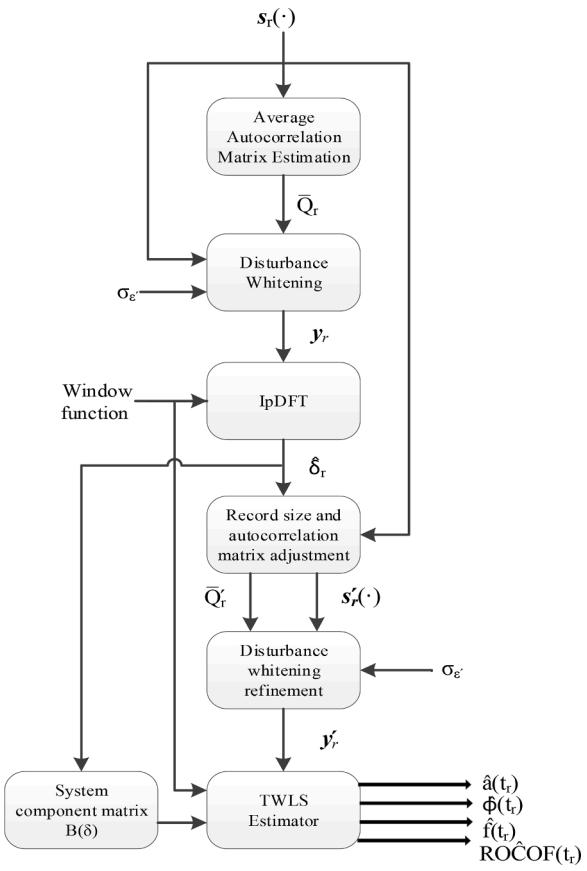

Fig. 1. Basic flowchart of the WI-TWLS algorithm for synchrophasor, frequency and ROCOF estimation.

goal of the adopted whitening technique is to replace all eigenvalues in $\widetilde{\Lambda}_0$ with lower dummy values $\sigma_{\varepsilon'}^2 \leq \sigma_{\varepsilon}^2$, so that the power spectral density of the resulting signal containsjust the fundamental term and a noise floor possibly with a lower level than the original one. In fact, the fundamental should not be affected by the whitening transformation.

It is important to emphasize that, even though in principle $\sigma_{\varepsilon'}^2$ could be set arbitrarily close to 0, in practice choosing an excessively small value of $\sigma_{\varepsilon'}^2$ is pointless, since the lower bound to the variance of the Q_r estimator depends on the number of available samples and, therefore, on the data record length which generally includes a non-integer number of periods of all narrowband components.

If $\boldsymbol{s}_{r\text{-}k}$ (for $k = 0, \ldots, K\text{-}1$) denotes the sequence of K subsequent data records shifted sample-by-sample, a classic consistent estimator of (6) is [42]

$$\widehat{Q}_r = \frac{1}{K}\sum_{k=0}^{K-1} \mathbf{s}_{r-k}\mathbf{s}_{r-k}^T, \tag{7}$$

where, here and in the following, "$\widehat{\cdot}$" means that the corresponding quantity is estimated. In stationary conditions, the variance of (7) decreases as K grows. Unfortunately, both the number of operations and the memory requirements of (7) also increase quadratically with K. Therefore, to keep both hardware requirements and processing latency reasonable, K can be set equal to N. To further reduce the Q_r estimation variance due to both wideband noise and the fact that a non-integer number of fundamental cycles are collected, a recursive, computationally efficient moving average of L subsequent values given by (7) is performed, i.e.

$$\overline{Q}_r = \overline{Q}_{r-1} + \frac{1}{L}(\widehat{Q}_r - \widehat{Q}_{r-L+1}). \tag{8}$$

Thus, if $\overline{S}_r$ and $\overline{\widetilde{\Lambda}}_0$ are the estimates of matrices of S_r and $\widetilde{\Lambda}_0$, respectively, (the eigenvalues of the fundamental component can be indeed easily identified and excluded from $\overline{\widetilde{\Lambda}}_0$because they certainly are the largest ones) it is shown in the Appendix of [38] that the vector of data $\boldsymbol{y}_r$ resulting from the linear transformation

$$\mathbf{y}_r = \overline{U}\mathbf{s}_r = \mathbf{x}_r + \boldsymbol{\eta}_r \text{ with } \overline{U} = \left(\overline{S}_r \begin{bmatrix} I_2 & 0 \\ 0 & \sigma_{\varepsilon'}\overline{\widetilde{\Lambda}}_0^{-\frac{1}{2}} \end{bmatrix} \overline{S}_r^T\right), \tag{9}$$

can be expressed as the sum of the N-long vector $\boldsymbol{x}_r$ (including the samples of the fundamental component centered at reference time t_r) and vector $\boldsymbol{\eta}_r$ which comprises the samples of the residual wideband noise with zero-mean and variance σ_{η}^2. It is important to emphasize that the elements of $\boldsymbol{\eta}_r$ do not depend on the wanted noise floor only, but also, and above all, on the uncertainty associated with $\overline{Q}_r$ estimation, which affects the elements of matrix $\overline{U}$as well. Hence,$\sigma_{\eta}^2 > \sigma_{\varepsilon'}^2$, but it can be hardly quantified a priori, since it also depends on the testing conditions, namely on the number and severity of the disturbances affecting the fundamental. In any case, σ_{η}^2 can be reduced by increasing the length L of the moving average filter (8).

3.2. Off-nominal frequency offset estimation

As briefly mentioned in Sections 1 and 2, in the second step of the algorithm, the classic IpDFT is applied to estimate any off-nominal static frequency deviation. Indeed, this technique is computationally lightweight and it can return accurate frequency estimates through closed-form expression when the rectangular or the Maximum Sidelobes Decay (MSD) windows are used [17]. If $Y_r(\bullet)$ denotes the N-point windowed DFT of $\boldsymbol{y}_r$, and this is computed around the C-th frequency bin at which the fundamental component should be located in nominal conditions, the fractional off-nominal frequency deviation $\widehat{\delta}_r$ within the rth data record can be estimated with the IpDFT with a rectangular window, by using the following closed-form expression [43]:

$$\begin{aligned}\widehat{\delta}_r &= \frac{\widehat{f}_0(t_r)}{f_{\text{nom}}} - 1 \\ &= \text{acos}\left(\frac{\alpha_1 Y_r(C) - \alpha_2 Y_r(C+1) - \alpha_3 Y_r(C+2) + \alpha_4 Y_r(C+1)}{\beta_1(Y_r(C+1) - Y_r(C+2)) - \beta_2(Y_r(C+1) - Y_r(C))}\right)\frac{f_s}{2\pi f_{\text{nom}}} \\ &\quad - 1,\end{aligned} \tag{10}$$

where $\alpha_1 = (1 + e^{-j4\pi C/N})e^{-j2\pi/N}$, $\alpha_2 = 1 + e^{-j4\pi(C+1)/N}$, $\alpha_3 = -1 - e^{-j4\pi(C+2)/N}$, $\alpha_4 = -(1 + e^{-j4\pi(C+1)/N})e^{-j2\pi/N}$, $\beta_1 = -2e^{-j2\pi(C+2)/N}$ and $\beta_2 = 2e^{-j2\pi(C+1)/N}$. If instead the 2-term MSD window (namely, the Hann window) is adopted, the fractional off-nominal frequency deviation $\widehat{\delta}_r$ within the rth data record is given by [17]

$$\widehat{\delta}_r = \frac{\widehat{f}_0(t_r)}{f_{\text{nom}}} - 1 = \begin{cases} \frac{1}{C}\left(\frac{\gamma_1 - 2}{1 + \gamma_1}\right) & |Y_r(C-1)| \geq |Y_r(C+1)| \\ \frac{1}{C}\left(\frac{2\gamma_2 - 1}{1 + \gamma_2}\right) & |Y_r(C-1)| < |Y_r(C+1)| \end{cases}, \tag{11}$$

where by $\gamma_1 = \frac{|W(C)|}{|W(C-1)|}$, $\gamma_2 = \frac{|W(C+1)|}{|W(C)|}$ and $W(\bullet)$ is the discrete-time Fourier transform of the chosen window. It is worth emphasizing that in the following, the off-nominal frequency value returned by (10) or (11) is used not only to adjust the data record length (both to whiten narrowband interferers and to estimate synchrophasors, as explained in Section 3.3), but also to compute the coefficients of the TWLS matrix (as described in Section 3.4).

3.3. Window length adjustment and whitening refinement

The aim of this step of the WI-TWLS estimator is either to select from $\boldsymbol{s}_r$ (if δ>0) or to append to $\boldsymbol{s}_r$ (if δ<0) the samples that are needed to process an integer number of actual fundamental periods. In the latter case some additional samples of (1) must be buffered in the acquisition stage. If [•] is the operator rounding the argument to the closest integer, we can denote with $N' = \left[\frac{N}{1+\delta}\right]$ or $N' = \left[\frac{N}{1+\delta}\right] + 1$ (depending on whether $\left[\frac{N}{1+\delta}\right]$ is odd or even) the odd number of input samples to be included into the adjusted vectors$'_r$. Quite importantly, while adding or removing the samples to/from the data record, the reference time still lies in the center of the adjusted data record to avoid possible phase delays in synchrophasor angle estimation. Thus, the size of matrix $\overline{U}$ in (9) must be adjusted accordingly and the resulting $N' \times N'$ matrix given by [38]

$$\overline{U}' = \overline{S}\begin{bmatrix} I_2 & 0 \\ 0 & \sigma_{\varepsilon'}\overline{\widetilde{\Lambda}}_0^{-\frac{1}{2}} \end{bmatrix}\overline{S}^{\text{T}}, \tag{12}$$

has to be used for the whitening transformation prior to synchrophasor estimation. In (12), the estimated eigenvectors matrix $\overline{S}$ and matrix $\overline{\widetilde{\Lambda}}'_0$ (which includes the singular values of all narrowband disturbances) result from the SVD of $\overline{Q}'_r$. This matrix is given by the moving average of the estimated autocorrelation matrices of $\mathbf{s}'_r$ as in (8). Therefore, by repeating the same steps mentioned above and explained in [38], the linear transformation for narrowband disturbance whitening becomes

$$\mathbf{y}'_r = \overline{U}'\mathbf{s}'_r \simeq \mathbf{x}'_r + \boldsymbol{\eta}'_r, \tag{13}$$

where $\mathbf{x}'_r$ is the vector including the N' samples of the ideal fundamental component centered at reference time t_r and $\boldsymbol{\eta}'_r$ is the vector including the residual zero-mean wideband noise samples. It is worth emphasizing that the variance σ_{η}^2 of $\boldsymbol{\eta}'_r$ is lower than or equal to σ_{η}^2 because the contributors to σ_{η}^2 due to non-coherent sampling become negligible when an

integer number of cycles of one or more periodic signal components is collected.

3.4. TWLS with system coefficients adjustment

As briefly mentioned in Section 2, the basic TWLS estimator is sensitive to low-orders harmonics and interharmonics over short observation intervals [36]. In addition, the accuracy of a basic TWLS estimator with the matrix coefficients computed at the nominal frequency degrades when off-nominal static frequency deviations occur. To overcome these two problems, not only the TWLS estimator is applied to $\mathbf{y}'_r$, but also the off-nominal frequency deviation estimated through (10) or (11) is used to tune the elements of the TWLS system matrix. Assuming to compute the Taylor's series of (3) at a time close to reference time t_r and to truncate the series to the second order (higher order coefficients have indeed a negligible impact on estimation accuracy [34]), it follows that [33]

$$p(n_r) = p(r+n) \approx p_{0,r} + p_{1,r}\, n + p_{2,r}\, n^2, \tag{14}$$

where $-\frac{N'-1}{2} \le n \le \frac{N'-1}{2}$, $p_{0,r} = p(t_r)$ as defined in (3), while coefficients $p_{1,r}$ and $p_{2,r}$ are proportional to the first and the second derivatives, respectively, of the dynamic phasor function computed at t_r, i.e., $p_{1,r} = \frac{1}{f_s}\frac{dp}{dt}|_{t_r}$ and $p_{2,r} = \frac{1}{2!f_s^2}\frac{d^2p}{dt^2}|_{t_r}$. If the Euler formulas are applied to the discrete-time fundamental component $x(t)$ in (1), by replacing (14) into the definition of synchrophasor, it follows that

$$x(n_r) \approx \frac{1}{\sqrt{2}}\left[\left(p_{0,r}+p_{1,r}n+p_{2,r}n^2\right)e^{j2\pi\left(\frac{1+\delta}{M}\right)n} + \left(p^*_{0,r}+p^*_{1,r}n+p^*_{2,r}n^2\right)e^{-j2\pi\left(\frac{1+\delta}{M}\right)n}\right], \tag{15}$$

where, here and in the following, the complex conjugate quantities are denoted with symbol "*". If the Taylor's series coefficients and their respective conjugate terms are arranged into a single column vector $\mathbf{p}_r = [p_{2,r}\ p_{1,r}\ p_{0,r}\ p^*_{0,r}\ p^*_{1,r}\ p^*_{2,r}]^T$, assuming that the Taylor's series truncation errors are negligible as compared with $\boldsymbol{\eta}'_r$, it follows from (15) that the rightmost side of (13) can be expressed as

$$\mathbf{y}'_r \approx B(\delta)\mathbf{p}_r + \boldsymbol{\eta}'_r, \tag{16}$$

where $B(\delta)$ is the $N' \times 6$ matrix defined as in [30], i.e.,

$$B(\delta) = \begin{bmatrix} \left(-\frac{N'-1}{2}\right)^2 e^{j\left(\frac{N'-1}{2}\right)\left(\frac{2\pi(1+\delta)}{M}\right)} & \left(-\frac{N'-1}{2}\right) e^{j\left(\frac{N'-1}{2}\right)\left(\frac{2\pi(1+\delta)}{M}\right)} & e^{j\left(\frac{N'-1}{2}\right)\left(\frac{2\pi(1+\delta)}{M}\right)} & e^{-j\left(\frac{N'-1}{2}\right)\left(\frac{2\pi(1+\delta)}{M}\right)} & \left(-\frac{N'-1}{2}\right) e^{-j\left(\frac{N'-1}{2}\right)\left(\frac{2\pi(1+\delta)}{M}\right)} & \left(-\frac{N'-1}{2}\right)^2 e^{-j\left(\frac{N'-1}{2}\right)\left(\frac{2\pi(1+\delta)}{M}\right)} \\ \vdots & \vdots & \vdots & \vdots & \vdots & \vdots \\ 0 & 0 & 1 & 1 & 0 & 0 \\ \vdots & \vdots & \vdots & \vdots & \vdots & \vdots \\ \left(\frac{N'-1}{2}\right)^2 e^{-j\left(\frac{N'-1}{2}\right)\left(\frac{2\pi(1+\delta)}{M}\right)} & \left(\frac{N'-1}{2}\right) e^{-j\left(\frac{N'-1}{2}\right)\left(\frac{2\pi(1+\delta)}{M}\right)} & e^{-j\left(\frac{N'-1}{2}\right)\left(\frac{2\pi(1+\delta)}{M}\right)} & e^{j\left(\frac{N'-1}{2}\right)\left(\frac{2\pi(1+\delta)}{M}\right)} & \left(\frac{N'-1}{2}\right) e^{j\left(\frac{N'-1}{2}\right)\left(\frac{2\pi(1+\delta)}{M}\right)} & \left(\frac{N'-1}{2}\right)^2 e^{j\left(\frac{N'-1}{2}\right)\left(\frac{2\pi(1+\delta)}{M}\right)} \end{bmatrix} \tag{17}$$

Ultimately, if the value of $\hat{\delta}_r$ returned by (10) or (11) is replaced to δ into $B(\delta)$ and assuming that the signal samples in $\mathbf{y}'_r$ are weighted by the chosen window function (for the reasons explained in Section 2), it follows that $\Omega\mathbf{y}'_r \approx \Omega B(\hat{\delta}_r)\mathbf{p}_r + \Omega\boldsymbol{\eta}'_r$, where Ω is a diagonal matrix including the coefficients of the window function. Thus, by solving the previous linear system of equations, the elements of vector $\boldsymbol{p}_r$ can be estimated as follows, i.e.

$$\hat{\mathbf{p}}_r = \left[B_r^H(\hat{\delta}_r)\Omega^2 B_r(\hat{\delta}_r)\right]^{-1} B_r^H(\hat{\delta}_r)\Omega^2\,\mathbf{y}'_r, \tag{18}$$

where superscript "^{H}" denotes the Hermitian operator and $\Omega^2 = \Omega^H \bullet \Omega$ because Ω is diagonal and real-valued.

Finally, it results from (18) that the amplitude, phase, frequency and ROCOF values of the fundamental component estimated at time t_r are given by [31]:

$$\hat{a}(t_r) = \sqrt{2}\left|\hat{p}_{0,r}\right|, \tag{19}$$

$$\hat{\varphi}(t_t) = \arg\left\{\hat{p}_{0,r}\right\}, \tag{20}$$

$$\hat{f}(t_r) = f_{\mathrm{nom}}(1+\hat{\delta}_r) + \frac{f_s}{2\pi\left|\hat{p}_{0,r}\right|^2}\mathrm{Im}\left\{\hat{p}_{1,r}\,\hat{p}^*_{0,r}\right\}, \tag{21}$$

$$\widehat{ROCOF}(t_r) = \frac{f_s^2}{\pi}\left\{\frac{\mathrm{Im}\left\{\hat{p}_{2,r}\,\hat{p}^*_{0,r}\right\}}{\left|\hat{p}_{0,r}\right|^2} - \frac{\mathrm{Re}\left\{\hat{p}_{1,r}\,\hat{p}^*_{0,r}\right\}\mathrm{Im}\left\{\hat{p}_{1,r}\,\hat{p}^*_{0,r}\right\}}{\left|\hat{p}_{0,r}\right|^4}\right\}. \tag{22}$$

Note that $Re\{\bullet\}$ and $\mathrm{Im}\{\bullet\}$ are real- and imaginary-part operators, respectively. Even if expressions (19)-(22) can be potentially used to return the quantities of interest anytime a new sample is acquired, in practice the stream of output measurement values has to be decimated to avoid a data tsunami as well to meet the PMU reporting rate requirements specified in the IEEE/IEC Standard. In this final decimation step, all the phasor parameters estimated within a single reporting period (except the phase angle which change linearly with time) can be averaged to further reduce the impact of the residual wideband noise, which is particularly critical for both frequency and ROCOF estimation [16].

4. Performance evaluation in P Class standard testing conditions

In this Section, the performance of the WI-TWLS algorithm is analyzed in depth through multiple Monte Carlo simulations in the *P Class* testing conditions specified in [11]. In particular, a twofold comparison is performed in the following. First, the benefits of the proposed approach in various testing conditions using one-cycle-long data records are shown and are compared with the results obtained with both the basic TWLS estimator and the TWLS algorithm enhanced by a preliminary narrowband disturbance whitening with no frequency adjustment [38] (briefly referred to as Whitening-based TWLS or WTWLS method in the rest of this paper). Then, a further side-by-side comparison between different estimators based on narrowband disturbance whitening (namely the WTWLS method, the proposed WI-TWLS approach and the recently proposed Tuned Whitening Taylor-Kalman Filter (TW-TKF) [30]) is presented .

Quite importantly, the basic TWLS and the WTWLS algorithm do not

include the preliminary fundamental frequency estimation step. As a consequence, neither data record length adjustment, nor TWLS system coefficients tuning can be performed. Moreover, in the WTWLS case the autocorrelation matrix used for narrowband disturbance whitening is estimated directly from (7) (as explained in [38]), i.e., without applying the moving average step conceived to reduce Q_f estimation uncertainty.

In all tests, the Root Mean Square (RMS) value of the fundamental is set equal to 1 p.u., $f_{nom} = 50$ Hz and $f_s = 5$ kHz. Therefore, $M = 100$ samples per nominal fundamental period are collected. Each test is repeated for different values of the most important parameters, such as off-nominal frequency deviation or interharmonic frequency. For every tuple of such parameters, the same test is repeated 100 times over 1-second–long intervals. The initial phase of all narrowband components is varied randomly in [-π, π] with uniform probability. Data records with a duration of either $C = 1$ or $C = 2$ fundamental periods are used in all tests in order to keep latency as low as possible. Thus, either $N = 100$ or $N = 200$ samples at a time are processed to return a single set of synchrophasor magnitude, phase, frequency and ROCOF values. In the former case, the plain rectangular window is used, whereas in the latter the Hann window is adopted both for fundamental frequency estimation through the IpDFT, and to build the weight matrix Ω in (17). The rectangular window is preferable for $C = 1$ because of the narrower spectral mainlobe width. The Hann window instead provides a good tradeoff in terms of both spectral resolution and spectral leakage suppression when 2 cycles are observed [36]. Moreover, it allows a lightweight closed-form implementation of the IpDFT, as confirmed by (11). In all simulations, the Signal-to-Noise Ratio (SNR) due to the white band noise $\epsilon(t)$ in (1) is set to 66 dB. This value corresponds to 11 effective bits and it is quite reasonable because, even if the nominal resolution of a PMU analog-to-digital converters usually ranges from 12 to 14 bits [44,45], the actual wideband noise is due not only to quantization, but also to further random phenomena that affect, for instance, instrument transformers and analog front-end circuitry (e.g., synchronization jitter and quantizer non-idealities). Both the values of K and L in (7) and (8) are set equal to N, to limit the computational burden. The noise floor power $\sigma^2_{\epsilon'}$ after whitening is instead computed in such a way that the maximum SNR of (13) is about 96 dB. As a last remark, it should be noted that the PMU reporting rate is assumed to be 50 frame/s. Therefore, the estimated values are decimated accordingly (see Section 3.3).

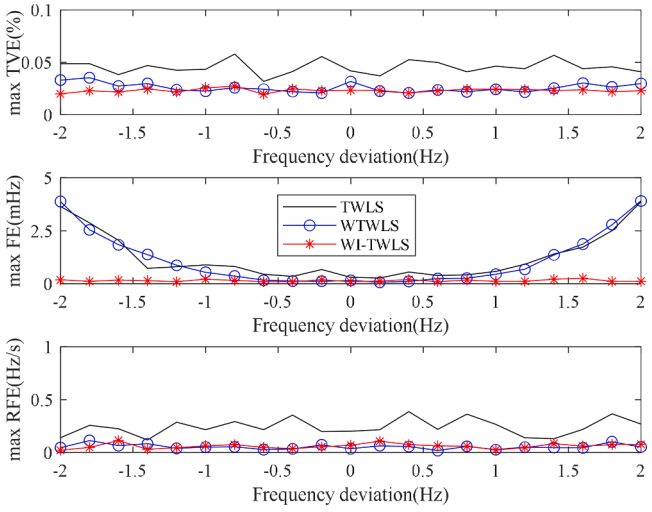

Fig. 2. Max. values of TVE, |FE| and |RFE| values returned by the TWLS, the WTWLS and the WI-TWLS estimators over one-cycle-long data records as a function of off-nominal frequency deviations compliant with the *P Class* requirements specified in the IEC/IEEE Standard when just the fundamental component is considered.

Table 1
Max. values of TVE, |FE| and |RFE| returned by the WTWLS, the WI-TWLS and the TW-TKF estimators for $C = 1$ (with a rectangular window) or $C = 2$ (with the Hann window) when off-nominal frequency offsets within ±2 Hz affect the fundamental component.

Error type	Standard limit	Algorithm	Data record length (in no. of power-line cycles) C = 1	C = 2
TVE_{max} [%]	1	WTWLS	0.04	0.02
		WI-TWLS	**0.02**	**0.02**
		TW-TKF	0.04	0.02
$\|FE\|_{max}$ [mHz]	5	WTWLS	3.9	6.8
		WI-TWLS	**0.2**	**0.08**
		TW-TKF	2.0	0.8
$\|RFE\|_{max}$ [Hz/s]	0.4	WTWLS	0.4	0.07
		WI-TWLS	**0.1**	**0.02**
		TW-TKF	0.5	0.05

4.1. Static frequency deviations and frequency ramp testing

The simplest P Class steady-state PMU test is performed by changing the fundamental frequency by at most ±2 Hz [11]. In Fig. 2 the maximum values of TVE, |FE| and |RFE| returned by the TWLS estimator, the WTWLS and the proposed WI-TWLS estimators over one-cycle-long data records (i.e., for $C = 1$) are plotted as a function of the static off-nominal frequency offset. The WI-TWLS algorithm outperforms the other estimators mainly because of the preliminary IpDFT-based frequency estimation.

Obviously, in this test the whitening transformation has just a marginal effect on accuracy improvement since no narrowband disturbances are considered in (1). Similar results can be obtained when $C = 2$, but the improvement is less visible. The comparison between different whitening-based techniques summarized in Table 1 reveals that the TVE, |FE| and |RFE| values obtained with the WI-TWLS technique are lower than those resulting from the application of both the WTWLS and the TW-TKF algorithms. It is worth noting that the results reported in Table 1 almost coincide with those obtained in the frequency ramp test. This test is implemented by increasing or decreasing linearly the fundamental frequency at the rate of ±1 Hz/s till reaching a maximum/minimum deviation of ±2 Hz. The TVE, |FE| and |RFE| values within the 40-ms-long time intervals at the beginning and at the end of each ramp are excluded from the analysis, in accordance with the IEEE/IEC Standard when the reporting rate is 50 frame/s [11]. The fact that the results obtained with off-nominal static frequency deviations and using linear frequency ramps almost coincide is not surprising. Indeed, for data records of a few cycles, a ROCOF of ±1 Hz/s causes a fundamental frequency shift of just a few tens of mHz.

4.2. Harmonic testing

Fig. 3 shows the maximum values of TVE, |FE| and |RFE| returned by the basic TWLS, the WTWLS and the WI-TWLS estimators over one-cycle-long intervals when the fundamental frequency deviation ranges from - 2 Hz to 2 Hz and with $D = 25$, 1 % narrowband harmonics in (2). It is clear that, even in the case of multiple interfering tones, the WI-TWLS is insensitive to both frequency deviations and number of harmonics. On the contrary, the TVE, |FE| and |RFE| values obtained with the original basic TWLS estimator are significant and they are mainly due to the lower orders harmonics.

The IEEE/IEC Standard prescribes that, in the *P Class* case, all harmonics from the 2nd to the 50th (one at a time) must be added to the fundamental component [11]. The amplitude of such harmonics must be equal to 1 % of the fundamental. Again, off-nominal relative frequency deviations within ± 2 Hz affect the fundamental and, consequently, all harmonics. Table 2 summarizes the results achieved with the WTLWS, the proposed WI-TWLS and the TW-TKF techniques over one-cycle-long and two-cycle data records respectively, along with the TVE, |FE| and |

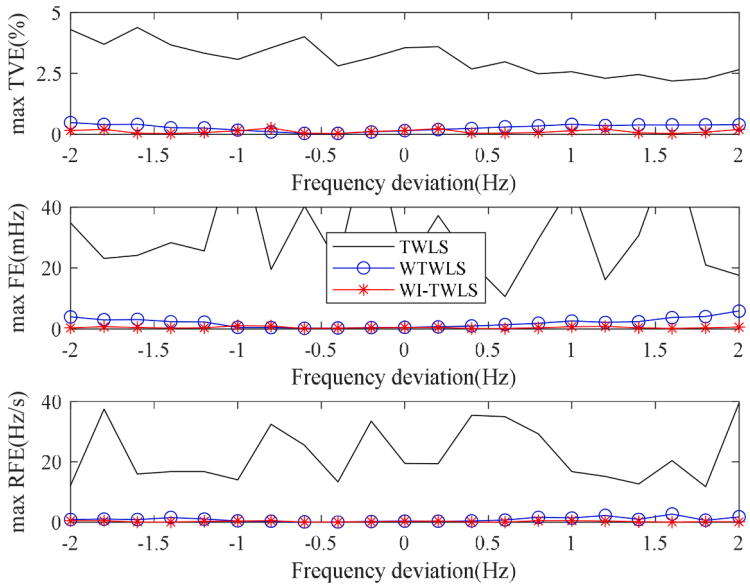

Fig. 3. Max. values of TVE, |FE| and |RFE| returned by the TWLS, the WTWLS and the WI-TWLS estimators over one-cycle-long data records for frequency deviations within ± 2 Hz under the effect of multiple harmonics. All harmonics till the 25th have amplitude equal to 1 % of the fundamental.

Table 2
Max. TVE, |FE| and |RFE| values returned by the WTWLS, the WI-TWLS and the TW-TKF estimators for $C = 1$ (with a rectangular window) or $C = 2$ (with the Hann window) under the effect of one harmonic at a time of amplitude equal to 1 % of the fundamental and with frequency offsets within ±2 Hz.

Error type	Standard limit	Algorithm	Data record length (in no. of power-line cycles)	
			C = 1	C = 2
TVE_{max} [%]	1	WTWLS	0.17	0.09
		WI-TWLS	**0.05**	**0.02**
		TW-TKF	0.04	0.02
$\|FE\|_{max}$ [mHz]	5	WTWLS	4.5	6.7
		WI-TWLS	**0.6**	**0.2**
		TW-TKF	2	0.8
$\|RFE\|_{max}$ [Hz/s]	0.4	WTWLS	0.5	0.05
		WI-TWLS	**0.1**	**0.01**
		TW-TKF	0.4	0.06

RFE| *P Class* limits specified in [9]. The obtained values give proof of the effectiveness of joint off-nominal frequency deviation compensation and harmonics whitening. Indeed, the estimation accuracy of the WI-TWLS algorithm is almost the same as in the off-nominal case only (see Table 1). Moreover, the results of Table 2 confirm the drastic accuracy improvement achievable with the WI-TWLS algorithm with respect to the WTWLS as well as the safe compliance with the *P Class* IEEE/IEC Standard limits even when $C = 1$. Quite importantly, the WI-TWLS and the TW-TKF algorithms return comparable results only when the TVE is considered. The maximum |FE| and |RFE| values obtained with the WI-TWLS technique are instead quite lower than the TW-TKF ones, especially when $C = 1$.

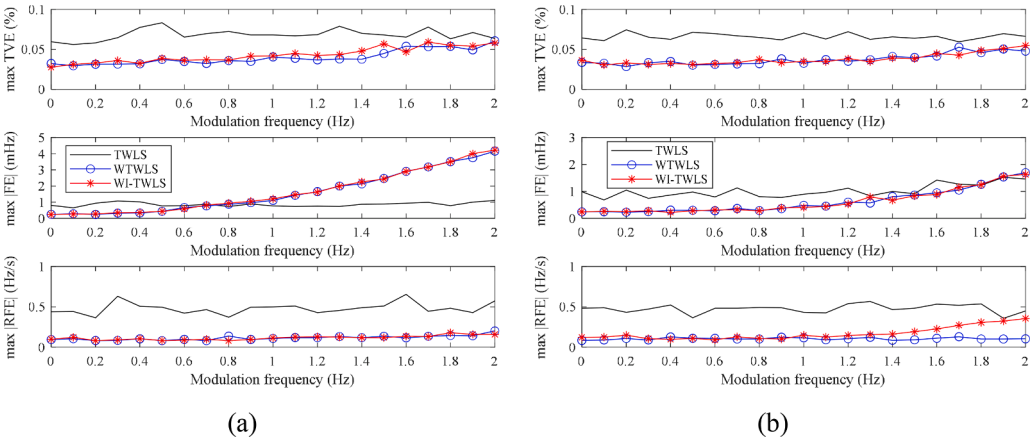

Fig. 4. Max. values of TVE, |FE| and |RFE| returned by the TWLS, the WTWLS and the WI-TWLS estimators over one-cycle-long data records as a function of the modulating sinewave frequency in the AM test (a) and the PM test (b), respectively. In both cases, the modulation index is 0.1.

4.3. Amplitude and phase modulation testing

As known, power systems oscillations can be roughly modeled through Amplitude Modulation (AM) and/or Phase Modulation (PM) signal models. The IEEE/IEC Standard prescribes that, in *P Class* testing conditions, a modulating sinewave of frequency up to 2 Hz and amplitude equal to 10 % of the fundamental (in the AM case) or 0.1 rad (in the PM case) affects the fundamental component. The effect of AM and PM on the TWLS, the WTWLS and the WI-TWLS algorithms over $C = 1$ data records is shown in Fig. 4(a) and 4(b), respectively, as a function of the modulating frequency. In both tests, the modulation index is 0.1. Note that the accuracy of the WTWLS and the WI-TWLS algorithms is almost the same (especially in the AM case). This is due to the fact that no off-nominal frequency needs to be estimated and compensated. For small modulating frequencies, the TVE, |FE| and |RFE| values are lower than those obtained with the basic TWLS algorithm, mainly because of the noise floor reduction caused by the disturbance whitening transformation. However, as the modulating tone frequency grows, the TVE, |FE| and |RFE| values obtained with the WTWLS and the WI-TWLS algorithms tend to increase, although at a different rate.

This trend is consistent with the preliminary results shown in [38] and it grows worse as the observation interval length grows. In fact, the more the narrowband disturbance whitening is effective, the more such a transformation smooths the amplitude and phase oscillations that the cascaded TWLS estimator is supposed to track. This is the main reason why the whitening-based techniques are not recommended over observation intervals longer than three or four fundamental periods. Such a performance degradation is particularly evident for frequency errors (especially in the AM case), because the smoothing errors caused by the whitening transformation affect (21) more strongly than the estimators of amplitude, phase and ROCOF.

Indeed, the whitening step tends to desensitize the inherent tracking capability of the basic TWLS algorithm, which is instead natively conceived to estimate amplitude, frequency and phase fluctuations over time. The comparison between the WTWLS, the WI-TWLS and the TW-TKF techniques for $C = 1$ and $C = 2$ data records under the effect of AM and PM oscillations (see Tables 3.A and 3.B) confirm that i) the WTWLS and WI-TWLS algorithms generally exhibit good accuracy under dynamic conditions (with the only exception of the ROCOF estimation in the PM case) and ii) accuracy degrades as the observation interval grows, as expected. However, the WI-TWLS algorithm returns more accurate frequency and ROCOF estimates than the TW-TKF described in [30], while ensuring full compliance to the P Class requirements even over one-cycle-long data records.

Table 3
Max. values of TVE, |FE| and |RFE| returned by the WTWLS, the WI-TWLS and the TW-TKF estimators for $C = 1$ (with a rectangular window) or $C = 2$ (with the Hann window) under the effect of amplitude (a) or phase modulation (b). In both cases the modulating signal is a 2-Hz sinewave and the modulation index is 0.1.

(A)

Error type	Standard limit	Algorithm	Data record length (in no. of power-line cycles) C = 1	C = 2
TVE_{max} [%]	3	WTWLS	0.06	0.08
		WI-TWLS	**0.06**	**0.07**
		TW-TKF	0.05	0.07
$\|FE\|_{max}$ [mHz]	60	WTWLS	4.2	4.3
		WI-TWLS	**4.3**	**4.4**
		TW-TKF	6.0	6.0
$\|RFE\|_{max}$ [Hz/s]	2.3	WTWLS	0.2	0.06
		WI-TWLS	**0.2**	**0.06**
		TW-TKF	0.4	0.6

(B)

Error type	Standard limit	Algorithm	Data record length (in no. of power-line cycles) C = 1	C = 2
TVE_{max} [%]	3	WTWLS	0.05	0.07
		WI-TWLS	**0.05**	**0.07**
		TW-TKF	0.05	0.07
$\|FE\|_{max}$ [mHz]	60	WTWLS	1.7	3.5
		WI-TWLS	**1.7**	**3.3**
		TW-TKF	26	49
$\|RFE\|_{max}$ [Hz/s]	2.3	WTWLS	0.1	0.05
		WI-TWLS	**0.4**	**0.05**
		TW-TKF	0.6	0.7

Table 4
Max. synchrophasor, frequency and ROCOF response times of the basic TWLS, the WTWLS, the proposed WI-TWLS, and the TW-TKF estimators for $C = 1$ (with a rectangular window) or $C = 2$ (with the Hann window) when either (a) ± 10 % amplitude steps or (b) ± π/18 phase Steps occur.

(A)

	Standard limit	Algorithm	No. of cycles C = 1	C = 2
Synchrophasor resp. time [cycles]	2	TWLS	1.01	1.41
		WTWLS	1.51	1.84
		WI-TWLS	**1.61**	**1.85**
		TW-TKF	1.55	2.83
Frequency resp. time [cycles]	4.5	TWLS	1.95	2.17
		WTWLS	2.66	3.77
		WI-TWLS	**2.31**	**3.77**
		TW-TKF	1.90	3.82
ROCOF resp. time [cycles]	6	TWLS	1.94	2.48
		WTWLS	2.89	4.13
		WI-TWLS	**2.67**	**4.13**
		TW-TKF	1.97	3.87

(B)

	Standard limit	Algorithm	No. of cycles C = 1	C = 2
Synchrophasor resp. time [cycles]	2	TWLS	0.91	1.68
		WTWLS	1.85	3.37
		WI-TWLS	**1.86**	**3.41**
		TW-TKF	1.81	3.37
Frequency resp. time [cycles]	4.5	TWLS	1.87	2.21
		WTWLS	2.69	3.84
		WI-TWLS	**2.70**	**3.94**
		TW-TKF	1.95	3.88
ROCOF resp. time [cycles]	6	TWLS	2.01	2.40
		WTWLS	2.93	4.11
		WI-TWLS	**2.91**	**4.28**
		TW-TKF	2.29	3.93

4.4. Amplitude and phase steps testing

Finally, the responsiveness of the TWLS estimator, the WTWLS algorithm, the proposed WI-TWLS technique and the TW-TKF estimator was analyzed and compared during transients. To that aim, the response times associated with synchrophasor, frequency and ROCOF estimation were evaluated. In the IEEE/IEC Standard, the *P Class* response times are the temporal intervals between the instants at which the TVE, |FE| or |RFE| values, due to an amplitude or a phase step change, exceed 1 %, 5 mHz or 0.4 Hz/s, respectively, and the times after which the TVE, |FE| or |RFE| patterns steadily remain under such thresholds.

The amplitude and phase step changes must be within ±10 % of the fundamental amplitude and within ±π/18, respectively. The

Table 5
Average execution times (per data record) of the four algorithms considered when $C = 1$ (with a rectangular window) and $C = 2$ (with the Hann window). In all cases, about $M = 100$ samples per fundamental period are processed.

Algorithm	Execution time per data record (ms) $C = 1$ (i.e. $N = 100$ samples)	$C = 2$ (i.e. $N = 200$ samples)
TWLS	0.85	1.25
WTWLS	3.82	12.22
WI-TWLS	**7.24**	**23.44**
TW-TKF	8.71	23.96

corresponding maximum response times, expressed in nominal cycles, are reported in Table 4.A and 4.B. The main conclusions that can be drawn from such results can be summarized as follows, i.e.

- In all cases, the whitening transformation increases the response times of the basic TWLS estimator. This is the price to pay to achieve higher accuracy. Nevertheless, in all cases, all response times are safely below the *P Class* limits when both amplitude and phase steps occur. In particular, when $C = 1$ the response times for synchrophasor estimation never exceed 2 cycles and those for frequency and ROCOF estimation are below 3 cycles.
- The response times over two-cycle-long data records are considerably longer than those obtained over one-cycle-long intervals, with no significant benefits in terms of estimation accuracy in other testing conditions.
- The responsiveness of the WTWLS and WI-TWLS techniques is quite comparable. This is reasonable, because neither the frequency tuning, nor the better disturbance whitening provided by the WI-TWLS have relevant effects on the spectrum of step-like changes. On the other hand, the TW-TKF estimator is faster in tracking the step changes, but it returns less accurate results.

4.5. Execution times

The average execution times of the proposed WI-TWLS technique with the settings described at the beginning of Section 4 and those of the other estimators considered for comparison are reported in Table 5. All algorithms were implemented in Matlab 2017b. The execution times (expressed in ms) were measured using a PC equipped with 16 GB of RAM and an AMD microprocessor Ryzen 7 4800H running at 2.90 GHz. The average values were computed over 1000 data records consisting of $C = 1$ or $C = 2$ cycles, respectively. The algorithms including the whitening step are clearly much slower than the basic TWLS technique due to the preliminary autocorrelation matrix estimation and the subsequent SVD computation, whose order of complexity is $O(N^3)$ [30]. The TW-TKF execution time is particularly high because the computational burden of the initial MUSIC algorithm for static frequency estimation also grows cubically with the data record size. In fact, this is much higher than the burden of the IpDFT approach adopted in this paper. Quite importantly, while the execution times over one-cycle-long intervals are reasonably shorter than one fundamental period (i.e., 20 ms at 50 Hz and 16.7 ms at 60 Hz), this is no longer true in the case of two-cycle-long data records. Although further performance improvement could be achieved by using a low-level software implementation (e.g., in C/C++ language), the reported results suggest that only for $C = 1$ a reporting rate of 50 or 60 measurements per second can be safely guaranteed if a mid- to high-end processing platform is adopted to run the algorithm. Considering also the results of the accuracy analysis reported in Sections 4.1–4.4, apparently there is no reason to process data records longer than one fundamental period at a time. Therefore, only the results over one-cycle-long data records will be considered in the rest of this paper.

5. Experimental results in real-world conditions

In this Section, two kinds of experimental data sets are used to evaluate the performance of the proposed algorithm both in the case of large steady-state harmonic distortion and during transient events.

5.1. Results under harmonic distortion exceeding the limits of the EN standard 50160:2010

The first data sets consist of multiple records of stationary synthetic waveforms (generated by a NI cRIO 9068 controller through an NI-9263 output analog module and acquired by an analog input module NI 9205 at $f_s = 6$ kSa/s) affected by larger harmonic disturbances than those reported in [11] for *P Class* PMUs. The Standard EN 50160:2010 specifies the voltage characteristics of the electricity distribution systems in Europe [46]. In particular, the voltage frequency must lie within [47 Hz, 52 Hz], the Total Harmonic Distortion (THD) must not exceed 8 % at both Medium-Voltage and Low-Voltage levels, and the magnitude of the first 25 harmonics must be smaller than individual thresholds ranging from 0.5 % to 6 % of the fundamental component [46]. To evaluate the performance of the algorithm under stressed conditions, the frequency of the waveforms used for testing is set to either to 47 Hz or 52 Hz, with random initial phase within $[0, 2\pi)$ and with amplitude of the 2nd to the 7th harmonic equal to 2 %, 5 %, 1 %, 6 %, 0.5 %, and 5 % of the fundamental component, respectively. As a result, the THD is equal to 9.4 % as in [14], i.e., higher than the limits reported in the EN Standard 50160:2010. No higher-order harmonics are included in the model, since they can be easily filtered by the TWLS algorithm [36]. The reference values for amplitude, phase, frequency, and ROCOF at the reference times in each one-cycle-long observation interval were reconstructed a posteriori, using a sine-fitting procedure over the whole data set [47].

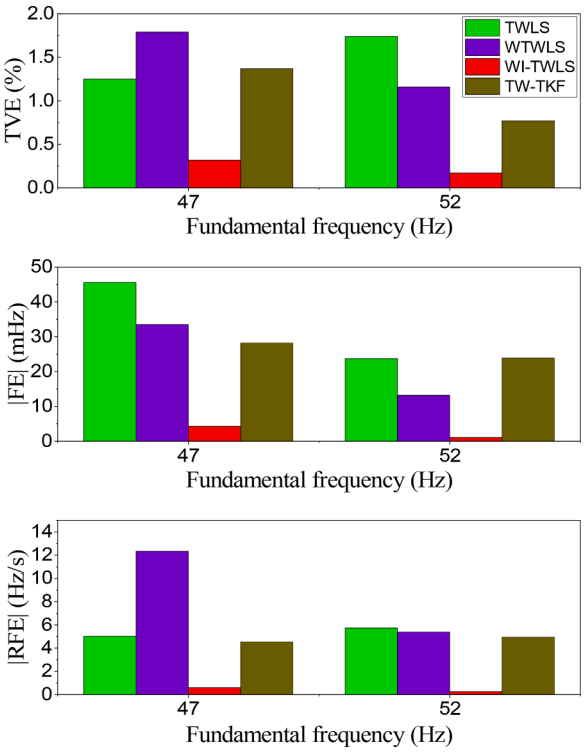

Fig. 5. Max. values of TVE, |FE| and |RFE| values returned by the TWLS estimator, the WTWLS variant, the newly proposed WI-TWLS technique and the TW-TKF dynamic estimator over one-cycle-long data records with multiple low order harmonics (THD = 9.4 %) and when the fundamental frequency is 47 Hz or 52 Hz, respectively.

The bar diagrams in Fig. 5 show the maximum values of TVE, |FE| and |RFE| returned by the TWLS estimator, the WTWLS variant, the newly proposed WI-TWLS technique and the previous TW-TKF dynamic estimator in the testing conditions described above. The results of Fig. 5 show clearly that the WI-TWLS algorithms outperforms the other reference algorithms. Quite importantly, TVE and |FE| are safely below 1 % and 5 mHz, respectively, while the |RFE| value is about 0.6 Hz/s for $f_1 = 47$ Hz and just about 0.25 Hz/s when $f_1 = 52$ Hz.

5.2. Results under real-world transient conditions

The second data set used for testing includes real-world 60-Hz three-phase waveforms sampled at $f_s = 15.360$ kHz (i.e., $M = 256$) affected by

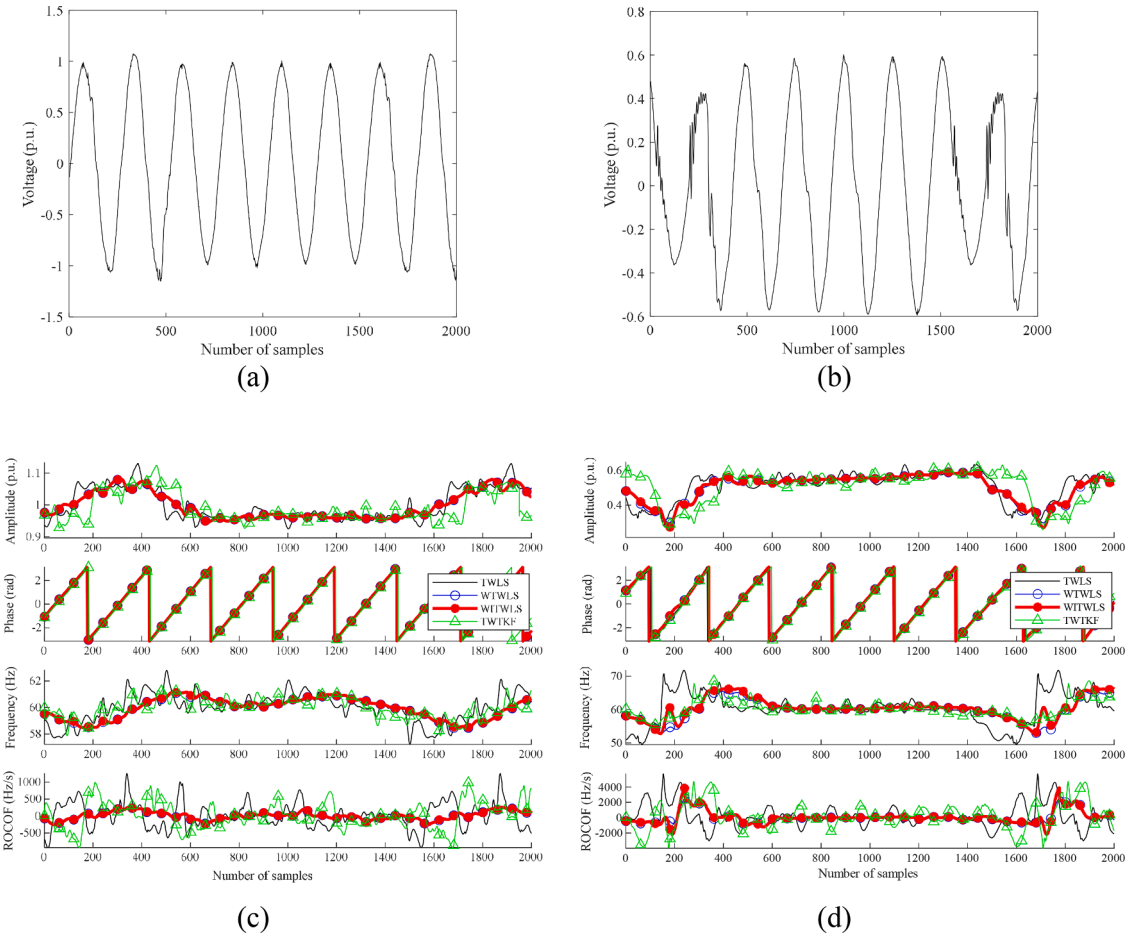

Fig. 6. (a)-(b): examples of experimental voltage waveforms affected by sudden events of different severity; (c)-(d): amplitude, phase, frequency and ROCOF patterns estimated with the TWLS estimator, the WTWLS variant, the newly proposed WI-TWLS technique and the TW-TKF dynamic estimator over one-cycle-long intervals in case (a) and (b), respectively.

a variety of visible short events, which cause sudden changes in amplitude, phase and/or frequency [48]. In this case, since the data are collected on the field (i.e., they are not synthetic), no ground-truth values of amplitude, phase, frequency and ROCOF are available, nor they can be determined with adequate accuracy. Nonetheless, a qualitative comparison between the basic TWLS estimator, the WTWLS variant, the newly proposed WI-TWLS technique and the previous TW–TKF dynamic estimator is shown in Fig. 6(a)–(d). In particular, Fig. 6(a)–(b) shows two examples of voltage waveforms affected by significant transient events, while Fig. 6(c)–(d) show the respective amplitude, phase, frequency and ROCOF patterns estimated by the various estimation algorithms over one-cycle-long intervals.

The event shown in Fig. 6(a) is a noticeable (but not too critical) joint amplitude and frequency oscillation, which is well tracked by both the WTWLS and the WI-TWLS estimators (whose results are basically overlapped), while the results returned by the basic TWLS and by the TW-TKF estimator are affected by evident and comparable fluctuations (see Fig. 6(c)). On the other hand, Fig. 6(b) shows two sudden one-cycle-long severe events occurring in an already strongly degraded scenario, as confirmed by the visible harmonic distortion and the reduction of voltage amplitude by about 40 % with respect to the nominal value. Again, the amplitude, phase, frequency and ROCOF values returned by the WTWLS and the WI-TWLS algorithms look trustworthy, and smoother than those obtained with the TW-TKF estimator, which nonetheless exhibits a more stable behavior than the basic TWLS technique. In conclusion, the lower supposed responsiveness of the whitening-based techniques during transients does not look critical in real operating conditions. At the same time, if one-cycle-long data records are considered, the WI-TWLS estimator certainly provides the highest rejection to harmonics.

6. Conclusions

The WI-TWLS algorithm described in this paper aims at improving *P Class* PMU measurement accuracy over short observation intervals. The proposed approach relies on the idea of i) whitening harmonics and interharmonics while reducing the signal noise floor and ii) compensating for the effect of possible frequency offsets, prior to computing synchrophasor magnitude and phase through a weighted least-squares estimator based on a Taylor's series synchrophasor model. The first part of the algorithm is very effective in mitigating the impact of steady-state narrowband interferers. The final Taylor-based weighted least squares estimator is instead supposed to track dynamic synchrophasor changes. Since this capability can be compromised by the preliminary whitening step, the best tradeoff is achieved over one-cycle-long data records when a rectangular window is used. This is also beneficial in terms of computational complexity. The tracking capability and responsiveness degradation with respect to the basic TWLS estimator or the Taylor-Kalman filter in transient conditions after sudden step-like events are tangible, but the IEEE/IEC Standard 60255–118–1–2018 requirements are met in any case. So, the worse responsiveness is acceptable and it is well counterbalanced by the resulting accuracy improvement. Some experimental results collected on the field confirm the simulation-based conclusions performed in the *P Class* testing conditions of the IEEE/IEC Standard 60255–118–1–2018.

CRediT authorship contribution statement

David Macii: Conceptualization, Methodology, Software, Writing – original draft. **Amir Bashian:** Methodology, Software, Validation, Writing – original draft. **Xuansheng Shan:** Data curation, Formal analysis, Software, Validation, Visualization. **Daniele Fontanelli:** Conceptualization, Methodology. **He Wen:** Funding acquisition, Supervision. **Dario Petri:** Conceptualization, Supervision.

Declaration of competing interest

The authors declare the following financial interests/personal relationships which may be considered as potential competing interests:

Xuansheng Shan reports that financial support was provided by the China Scholarship Council and by the National Key Research and Development Program of China (Grant no. 2022YFF0607700).

Data availability

Data will be made available on request.

References

[1] P.M. Joshi, H.K. Verma, Synchrophasor measurement applications and optimal PMU placement: a review, *Electr. Power Syst. Res.* 199 (2021), https://doi.org/10.1016/j.epsr.2021.107428 art. no. 107428.

[2] A. Mouco, A. Abur, Improving the wide-area PMU-based fault location method using ordinary least squares estimation, *Electr. Power Syst. Res.* 189 (2020), https://doi.org/10.1016/j.epsr.2020.106620 art. no. 106620Dec.

[3] J.J. Chavez, et al., PMU-voltage drop based fault locator for transmission backup protection, *Electr. Power Syst. Res.* 196 (2021), https://doi.org/10.1016/j.epsr.2021.107188 art. no. 107188.

[4] R.L.A. Reis, F.V. Lopes, E.J.S. Leite, G. Zat, J.V. Souza, A. Scheid, T.G. Jahn, Evaluation of single-ended impedance-based transmission fault location using fixed and variable window phasor estimation approaches, *Electr. Power Syst. Res.* 223 (2023), https://doi.org/10.1016/j.epsr.2023.109571.

[5] A. Bashian, M. Assili, A. Anvari-Moghaddam, A security-based observability method for optimal PMU-sensor placement in WAMS, *Int. J. Electr. Power Energy Syst.* 121 (2020) 106157, https://doi.org/10.1016/j.ijepes.2020.106157. Oct.

[6] R. Andreoni, D. Macii, M. Brunelli, D. Petri, Tri-Objective Optimal PMU Placement including Accurate State Estimation: the Case of Distribution Systems, IEEE Access 9 (2021) 62102–62117, https://doi.org/10.1109/ACCESS.2021.3074579.

[7] G. Barchi, D. Macii, A photovoltaics-aided interlaced extended Kalman filter for distribution systems state estimation, Sustain. Energy, Grids Networks 26 (2021) 100438, https://doi.org/10.1016/J.SEGAN.2021.100438. Jun.

[8] B. Gou, R.G. Kavasseri, Unified PMU placement for observability and bad data detection in state estimation, IEEE Trans. Power Syst. 29 (6) (2014) 2573–2580, https://doi.org/10.1109/TPWRS.2014.2307577. Nov.

[9] S. Afrandideh, F. Haghjoo, A DFT-based phasor estimation method robust to primary and secondary decaying DC components, *Electr. Power Syst. Res.* 208 (2022), https://doi.org/10.1016/j.epsr.2022.107907 art. no. 107907.

[10] I. Biyya, Z. Oubrahim, A. Abbou, Frequency and ROCOF estimation under steady-state and dynamic conditions for three-phase grid-connected converters, *Electr. Power Syst. Res.* 224 (2023), https://doi.org/10.1016/j.epsr.2023.109723 art. no. 109723.

[11] IEC/IEEE 60255-118-1:2018, *IEEE/IEC International Standard - Measuring relays and protection equipment - Part 118-1: synchrophasor for power systems - Measurements*, pp. 1–78, 2018.

[12] W. Meng, X. Wang, Z. Wang, I. Kamwa, Impact of Causality on Performance of Phasor Measurement Unit Algorithms, IEEE Trans. Power Syst. 33 (2) (2018) 1555–1565, https://doi.org/10.1109/TPWRS.2017.2734662.7. Mar.

[13] D. Macii, D. Petri, Digital filters for phasor measurement units: design criteria, advantages and limitations, in: 2019 *IEEE 10th International Workshop on Applied Measurements for Power Systems* (AMPS), Aachen, Germany, 2019, https://doi.org/10.1109/AMPS.2019.8897796. Sep.

[14] D. Macii, D. Belega, D. Petri, IpDFT-Tuned Estimation Algorithms for PMUs: overview and Performance Comparison, Appl. Sci. 11 (5) (2021) 2318, https://doi.org/10.3390/app11052318. Mar.

[15] F. Messina, L.R. Vega, P. Marchi, C.G. Galarza, Optimal differentiator filter banks for PMUs and their feasibility limits, IEEE Trans. Instr. Meas. 66 (11) (2017) 2948–2956, https://doi.org/10.1109/TIM.2017.2728378. Nov.

[16] D. Macii, D. Fontanelli, G. Barchi, D. Petri, Impact of acquisition wideband noise on synchrophasor measurements: a design perspective, *IEEE Trans. Instrum. Meas.* 65 (10) (2016) 2244–2253, https://doi.org/10.1109/TIM.2016.2594023. Oct.

[17] A. Karpilow, A. Derviškadić, G. Frigo, M. Paolone, Step detection in power system waveforms for improved RoCoF and frequency estimation, *Electr. Power Syst. Res.* 212 (2022), https://doi.org/10.1016/j.epsr.2022.108527 art. no. 108527Nov.

[18] D. Belega, D. Petri, Accuracy analysis of the multicycle synchrophasor estimator provided by the interpolated DFT algorithm, IEEE Trans. Instr. Meas. 62 (5) (2013) 942–953, https://doi.org/10.1109/TIM.2012.2236777.

[19] A. Derviškadić, M. Paolone, Design and experimental validation of an FPGA-based PMU simultaneously compliant with P and M performance classes, *Electr. Power Syst. Res.* 189 (2020) 106650, https://doi.org/10.1016/j.epsr.2020.106650. Dec.

[20] J. Song, A. Mingotti, J. Zhang, L. Peretto, H. Wen, Fast Iterative-Interpolated DFT Phasor Estimator Considering Out-of-Band Interference, IEEE Trans. on Instr. and Meas. 71 (2022) 1–14, https://doi.org/10.1109/TIM.2022.3203459. Art no. 9005814.

[21] D. Petri, D. Fontanelli, D. Macii, A frequency-domain algorithm for dynamic synchrophasor and frequency estimation, IEEE Trans. Instr. Meas. 63 (10) (2014) 2330–2340, https://doi.org/10.1109/TIM.2014.2308996. Oct.

[22] M. Bertocco, G. Frigo, C. Narduzzi, C. Muscas, P.A. Pegoraro, Compressive sensing of a taylor-fourier multifrequency model for synchrophasor estimation, IEEE Trans. Instr. Meas. 64 (12) (2015) 3274–3283, https://doi.org/10.1109/TIM.2015.2450295. Dec.

[23] J. Khodaparast, A review of dynamic phasor estimation by non-linear kalman filters, IEEE Access 10 (2022) 11090–11109, https://doi.org/10.1109/ACCESS.2022.3146732.

[24] L. Fu, L. Yu, S. Xiong, Z. He, R. Mai, X. Li, A dynamic synchrophasor estimation algorithm considering out-of-band interference, IEEE Trans. on Power Delivery 37 (2) (2022) 1193–1202, https://doi.org/10.1109/TPWRD.2021.3079990.

[25] H. Novanda, P. Regulski, F.M. González-Longatt, V. Terzija, Unscented kalman filter for frequency and amplitude estimation, in: IEEE PowerTech, Trondheim, Norway, 2011, pp. 1–6, https://doi.org/10.1109/PTC.2011.6019414.

[26] P. Regulski, V. Terzija, Estimation of frequency and fundamental power components using an unscented kalman filter, IEEE Trans. on Instr. Meas. 61 (4) (2012) 952–962, https://doi.org/10.1109/TIM.2011.2179342.

[27] Y. Lee, G. Lee, A. White, Y.-J. Shin, Oscillation parameter estimation via state-space modeling of synchrophasors, IEEE Trans. on Power Syst. (2024), https://doi.org/10.1109/TPWRS.2023.3332248 in-print.

[28] D. Fontanelli, D. Macii, D. Petri, Dynamic synchrophasor estimation using Smoothed Kalman filtering, in: Proc. *IEEE Int. Instr. and Meas. Tech. Conf. Proceedings*, Taipei, Taiwan, 2016, pp. 1–6, https://doi.org/10.1109/I2MTC.2016.7520462.

[29] J.A. de la O Serna, J. Rodríguez-Maldonado, Taylor–Kalman–Fourier Filters for Instantaneous Oscillating Phasor and Harmonic Estimates, IEEE Trans. on Instr. and Meas. 61 (4) (2012) 941–951, https://doi.org/10.1109/TIM.2011.2178677.

[30] A. Bashian, D. Macii, D. Fontanelli, D. Petri, A Tuned Whitening-Based Taylor-Kalman Filter for P Class Phasor Measurement Units, IEEE Trans. on Instr. and Meas. 71 (2022) 1–13, https://doi.org/10.1109/TIM.2022.3162274. Art no. 9002913.

[31] M.A. Platas-Garza, J.A. De La O Serna, Dynamic phasor and frequency estimates through maximally flat differentiators, *IEEE Trans. Instrum. Meas.* 59 (7) (2010) 1803–1811, https://doi.org/10.1109/TIM.2009.2030921. Jul.

[32] M.A. Platas-Garza, J.A. De La O Serna, Dynamic harmonic analysis through Taylor-Fourier transform, IEEE Trans. Instr. Meas. 60 (3) (2011) 804–813, https://doi.org/10.1109/TIM.2010.2064690. Mar.

[33] J.A. de la O Serna, Dynamic phasor estimates for power system oscillations, *IEEE Trans. Instrum. Meas.* 56 (5) (2007) 1648–1657, https://doi.org/10.1109/TIM.2007.904546. Oct.

[34] G. Barchi, D. Macii, D. Petri, Synchrophasor estimators accuracy: a comparative analysis, IEEE Trans. Instr. Meas. 62 (5) (2013) 963–973, https://doi.org/10.1109/TIM.2012.2236776.

[35] Ž. Zečević, I. Jokić, T. Popović, B. Krstajić, An efficient phasor and frequency estimation algorithm for wide frequency range, *Electr. Power Syst. Res.* 180 (106124) (2020), https://doi.org/10.1016/j.epsr.2019.106124. Mar.

[36] P. Tosato, D. Macii, M. Luiso, D. Brunelli, D. Gallo, C. Landi, A Tuned Lightweight Estimation Algorithm for Low-Cost Phasor Measurement Units, IEEE Trans. Instr. Meas. 67 (5) (2018) 1047–1057, https://doi.org/10.1109/TIM.2017.2775458. May.

[37] P. Stoica, A. Eriksson, MUSIC estimation of real-valued sine-wave frequencies, Signal Proc. 42 (2) (1995) 139–146, https://doi.org/10.1016/0165-1684(94)00123-H. Mar.

[38] D. Macii, G. Barchi, D. Fontanelli, Decorrelation-based harmonic distortion reduction for synchrophasor measurements, in: *AMPS 2017 - IEEE International Workshop on Applied Measurements for Power Systems*, Liverpool, UK, 2017, pp. 1–6, https://doi.org/10.1109/AMPS.2017.8078321.

[39] A.J. Roscoe, I.F. Abdulhadi, G.M. Burt, P and M Class Phasor Measurement Unit Algorithms Using Adaptive Cascaded Filters, IEEE Trans. on Power Deliv. 28 (3) (2013) 1447–1459, https://doi.org/10.1109/TPWRD.2013.2238256. July.

[40] M. Pramanik, A. Routray, P. Mitra, A two-stage adaptive symmetric-strong-tracking square-root cubature Kalman filter for harmonics and interharmonics estimation, *Electr. Power Syst. Res.* 210 (108133) (2022), https://doi.org/10.1016/j.epsr.2022.108133. Sep.

[41] K. Chauhan, R. Sodhi, A distribution-level PMU enabled Teager-Kaiser energy based islanding detector, Electric Power Syst. Res. 192 (2021), https://doi.org/10.1016/j.epsr.2020.106964 art. no. 106964.

[42] S.M. Kay, Fundamentals of Statistical Signal Processing: Estimation Theory, Prentice-Hall, Upper Saddle River, NJ, USA, 1993.

[43] K. Wang, H. Wen, G. Li, Accurate frequency estimation by using three-point interpolated discrete fourier transform based on rectangular window, IEEE Trans. on Ind. Inf. 17 (1) (2021) 73–81, https://doi.org/10.1109/TII.2020.2981542. Jan.

[44] A.D. Femine, D. Gallo, C. Landi, M. Luiso, The design of a low cost phasor measurement unit, Energies 12 (14) (2019) 2648, https://doi.org/10.3390/EN12142648, vol. 12Jul.
[45] D.M. Laverty, R.J. Best, P. Brogan, I. Al Khatib, L. Vanfretti, D.J. Morrow, The OpenPMU platform for open-source phasor measurements, IEEE Trans. Instr. Meas. 62 (4) (2013) 701–709, https://doi.org/10.1109/TIM.2013.2240920.
[46] EN 50160:2010, Voltage characteristics of electricity supplied by public distribution systems, brussels, Belgium, Dec. 2010.
[47] G. Simon, R. Pintelon, L. Sujbert, J. Schoukens, An efficient nonlinear least square multisine fitting algorithm, IEEE Trans. Instr. Meas. 51 (4) (2002) 750–755, https://doi.org/10.1109/TIM.2002.803304.
[48] Y.H. Gu, M.H.J. Bollen, Time-frequency and time-scale domain analysis of voltage disturbances, IEEE Trans. on Power Delivery 15 (4) (2000) 1279–1284, https://doi.org/10.1109/61.891515. Oct.